ACS OMEGA

Open Access

http://pubs.acs.org/journal/acsodf

Article

Reassignment of the Photoelectron Spectrum of Methylketene Using a Hybrid Model of Harmonic and Anharmonic Oscillators to Compute Franck–Condon Factors

Jia-Lin Chang,* Hsiang-Yu Chen, and Yun-Jhu Huang

Cite This: *ACS Omega* 2023, 8, 40685−40694

Read Online

ACCESS | Metrics & More | Article Recommendations | Supporting Information

ABSTRACT: We constructed a hybrid model of harmonic and anharmonic oscillators to compute Franck−Condon factors and interpret the photoelectron spectrum of methylketene. The equilibrium structures of methylketene and its cation were optimized, and then, the harmonic and anharmonic vibrational frequencies were computed using the B3LYP, PBE0, APFD, and ωB97XD approaches of the density functional theory. The photoelectron spectrum of methylketene was simulated by computing the Franck−Condon factors with both the harmonic and hybrid models. The adiabatic ionization energy of methylketene was computed by using the CCSD(T) approach extrapolating to the complete basis set limit. The simulated photoelectron spectra are consistent with those from the experiment for both the harmonic and hybrid models. However, the error in band positions is reduced by using the hybrid model. The computed adiabatic ionization energies of methylketene are in agreement with the experiment, with the smallest error being 0.017 eV. Our interpretation based on the theoretical spectrum led to the reassignment of the experimental photoelectron spectrum of methylketene.

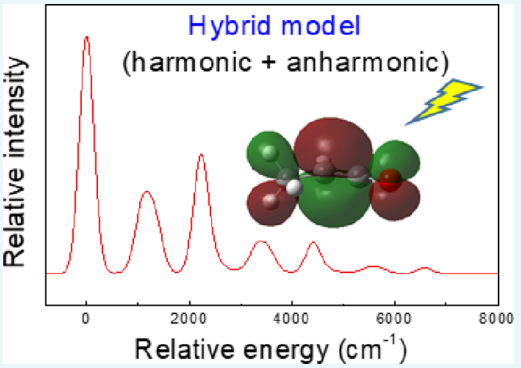

INTRODUCTION

Since the first astronomical observation of ketene ($H_2C{=}C{=}O$) in the interstellar medium,[1] the search of methylketene (MK) in space followed.[2] MK is regarded as a promising interstellar molecule to be detected because its energy is computed to be only slightly higher than *trans*-acrolein, the most stable isomer of C_3H_4O.[2−4] Given that *trans*-acrolein has been observed in some interstellar mediums,[5−8] it is anticipated that MK can also be detected. This line of thinking is consistent with the minimum energy principle based on thermodynamics, which describes that the abundance ratios of isomers in space are related to their energy differences.[9−11] Consequently, the more stable the isomer is, the more likely it is to be observed in the interstellar medium. However, to the best of our knowledge, the successful observation of interstellar MK has not yet been reported.

The unsuccessful hunt for MK in space has been interpreted by some research studies. For instance, based on computed potential energy surfaces, Field-Theodore and Taylor proposed that the lack of MK in interstellar space is owing to high activation energies and unfavorable kinetics.[4] Based on photoionization experiments, Derbali et al. proposed that MK might be hydrogenated or photoionized in the interstellar environment such that its abundance it too low to be detected.[12] In addition to the astronomical studies, MK is also of interest in the fields of spectroscopy,[12−16] theoretical computation,[17−21] photodissociation dynamics,[22−26] etc.

This study was inspired by Derbali et al. for their experimental and theoretical investigation of the photoelectron spectrum (PES) of MK.[12] The spectrum measured by Derbali et al. is of the highest resolution for the PES of MK reported up to date.[12,16] Derbali et al. also simulated the PES of MK by computing Franck−Condon factors (FCFs), and they found that the simulated spectrum was in agreement with the experiment.[12] However, instead of assigning the PES according to the FCF computation, they assigned the spectrum based on computations of anharmonic vibrational frequencies. Their strategy inspired our interest to compare two approaches for interpreting the vibronic spectrum of molecules. The first approach is to assign the peaks to the transitions whose vibrational frequencies are closest to the observed excitation energies, which is called the frequency approach (FA) in this study. The other approach is to assign the peaks to the transitions whose computed spectral patterns, including both intensities and excitation energies, are consistent with the observations. We call this the spectral approach (SA). Derbali et al. adopted the FA to assign the PES of MK, and we

Received: August 5, 2023
Accepted: October 2, 2023
Published: October 17, 2023

examined in this study whether the assignments between the FA and SA are in agreement with each other.[12]

A variety of approaches for computing FCFs has been reported in the literature. The harmonic-oscillator model is a good approximation for molecular vibrations not undergoing large-amplitude motions. Two harmonic oscillators are termed as "displaced" if their equilibrium geometries differ and "distorted" if the shapes of their potential energy curves, and consequently the vibrational frequencies, differ. For diatomic molecules which possess only one vibrational mode, the approaches for computing FCFs using the displaced and distorted harmonic-oscillator model are well documented.[27−31] The one-dimensional FCF formulas can also be applied to study the vibronic spectra of polyatomic molecules if the vibrational normal modes are assumed to be parallel between two electronic states. In this approximation, the FCF of a given transition is the product of the FCFs of all the individual modes. For polyatomic molecules, however, the normal coordinates between two electronic states might be rotated with respect to each other in addition to being displaced and distorted. Consequently, the Duschinsky effect,[32] which describes the mixing of normal coordinates arising from geometrical changes, must be taken into account. This problem has been tackled by different solutions.[33−42] Approaches for simulating vibronic spectra incorporating the Herzberg−Teller effect,[43] which is essential for symmetry-forbidden transitions, are also available.[40,44,45] In addition, different approaches for computing FCFs using the anharmonic-oscillator model have been reported.[46−51] However, owing to the high demand of computational cost, the anharmonic approaches of FCF theory are applicable only to molecules composed of a few atoms.

In the past decade, we have developed some approaches for computing FCFs of harmonic oscillators.[41,52−55] The Duschinsky effect[32] has been taken into account in our model for polyatomic molecules.[41] Our harmonic model for computing FCFs has been successfully applied to the studies of the PES of some molecules.[56−59] However, the excitation energies computed by the harmonic model are usually larger than the experimental values. Accordingly, we constructed a hybrid model of harmonic and anharmonic oscillators to compute the FCFs and simulate the vibronic spectra of the molecules in this study. In the hybrid model, the excitation energies are computed from the vibrational frequencies of anharmonic oscillators. The vibrational wave functions are still harmonic, but the vibrational frequencies in the expression of wave functions are replaced by the fundamental frequencies of anharmonic oscillators. In this regard, both the excitation energies and spectral intensities are partially corrected for the anharmonicity of molecular vibrations in the hybrid model. Similar approaches have been reported by Barone and co-workers.[45,60−63] The primary difference between our and their approaches is how the anharmonicity is implemented in the computation of FCFs. Barone and co-workers compute the FCF of excited vibrational states from recursive formulas, and the anharmonic frequencies are used in the recursive formulas.[62] In contrast, the FCF of each transition is computed using analytical formulas, and the wave functions corrected for anharmonicity are used directly for computing FCFs in our model (*vide infra*).

We simulated the PES of MK using both the harmonic and hybrid models and found that both models performed well in predicting the PES of MK. However, the error of excitation energies can be reduced by the hybrid model. Most importantly, our reassignment of the PES of MK using the SA is different from that of Derbali et al. using the FA.[12] We propose that the SA is superior to the FA for the interpretation of vibronic spectra of molecules.

THEORETICAL METHODS

Theory. The theory of the hybrid model is modified from our harmonic model for computing FCFs,[41] which is outlined briefly as follows. The Franck−Condon integral (FCI) for a vibronic transition between two harmonic oscillators with n vibrational modes in each can be written as

$$\begin{aligned}&\langle v_1 v_2 \cdots v_n | v_1' v_2' \cdots v_n' \rangle \\ &= N \int_{-\infty}^{\infty} \cdots \int_{-\infty}^{\infty} \prod_{i=1}^{n} H_{v_i}(\sqrt{\alpha_i} Q_i) H_{v_i'}(\sqrt{\alpha_i'} Q_i') \\ &\quad \exp\left(-\frac{1}{2}\alpha_i Q_i^2 - \frac{1}{2}\alpha_i' Q_i'^2\right) \mathrm{d}Q_i \end{aligned} \tag{1}$$

where v and v' are vibrational quantum numbers of the two electronic states, respectively, N is the product of normalization constants of the two harmonic oscillators, H_{v_i} is the Hermite polynomial, Q_i represents the normal coordinate, and

$$\alpha_i = \frac{\omega_i}{\hbar} \tag{2}$$

where ω_i is the angular frequency of the ith mode of the harmonic oscillator and $\hbar$ is Planck's constant divided by 2π. In the harmonic model, ω_i's are obtained from the computations of the vibrational frequencies of harmonic oscillators. In the hybrid model, all ω_i's are replaced with the angular frequencies of the fundamental bands of the anharmonic oscillators. To solve eq 1, which is the overlap integral of vibrational wave functions of two electronic states, the normal coordinates $\boldsymbol{Q}'$ are expressed as linear combinations of $\boldsymbol{Q}$,

$$\boldsymbol{Q}' = \boldsymbol{J}\boldsymbol{Q} + \boldsymbol{D} \tag{3}$$

where

$$\boldsymbol{J} = \boldsymbol{L}'\boldsymbol{L}^T \tag{4}$$

is the Duschinsky matrix, $\boldsymbol{L}$ is the displacement matrix of normal modes, and $\boldsymbol{L}^T$ is the transpose of the $\boldsymbol{L}$ matrix. In eq 3, $\boldsymbol{D}$ is the shift vector describing the change of equilibrium geometries between the two electronic states,

$$\boldsymbol{D} = \boldsymbol{L}'\boldsymbol{M}^{1/2}(\boldsymbol{X}_0 - \boldsymbol{X}_0') \tag{5}$$

where $\boldsymbol{M}$ is a matrix composed of atomic masses for the diagonal elements and zeros for off-diagonal elements, and $\boldsymbol{X}_0$ is the Cartesian coordinates of the equilibrium structure. Then, the arguments of the exponential function and the variables of the Hermite polynomials in eq 1 are transformed to new variables x_i by

$$x_i = Q_i + \sum_{j=i+1}^{n} B_{ij} Q_j + C_i \tag{6}$$

and

$$Q_i = x_i + \sum_{j=i+1}^{n} B_{ij}' x_j + C_i' \tag{7}$$

With such transformations, eq 1 becomes

https://doi.org/10.1021/acsomega.3c05750
ACS Omega 2023, 8, 40685−40694

$$\langle v_1 v_2 \cdots v_n | v_1' v_2' \cdots v_n' \rangle = NE \times \int_{-\infty}^{\infty} \cdots \int_{-\infty}^{\infty} \prod_{i=1}^{n} H_{v_i}\left(\sum_{j=i}^{n} a_{ij} x_j + d_i \right) H_{v_i'}\left(\sum_{j=1}^{n} a_{ij}' x_j + d_i' \right) \exp(-A_i x_i^2) \mathrm{d}x_i \quad (8)$$

where

$$E = \exp\left(-\frac{1}{2} \sum_{i=1}^{n} \alpha_i' D_i^2 + \sum_{i=1}^{n} A_i C_i^2 \right) \quad (9)$$

By expanding the Hermite polynomials in eq 8 using the following equation repeatedly,

$$H_n(x + d) = \sum_{k=0}^{n} \binom{n}{k} H_{n-k}(d)(2x)^k \quad (10)$$

the integrals in eq 8 can be transformed to the products of Gaussian integrals, which can be solved using

$$\int_{-\infty}^{\infty} x^{2s} \exp(-ax^2) \mathrm{d}x = \frac{(2s-1)!!}{2a^s} \left(\frac{\pi}{a}\right)^{1/2} \quad (11)$$

Finally, the general formula of FCI for harmonic oscillators with arbitrary dimensions is derived as

$$\langle v_1 v_2 \cdots v_n | v_1' v_2' \cdots v_n' \rangle = \frac{HI_0}{V} \quad (12)$$

where

$$I_0 = \langle 00 \cdots 0 | 00 \cdots 0 \rangle = E \left(\prod_{i=1}^{n} \frac{\sqrt{\alpha_i \alpha_i'}}{A_i} \right)^{1/2} \quad (13)$$

is the FCI of the adiabatic transition,

$$V = \left[\prod_{i=1}^{n} (2^{v_i + v_i'} v_i! v_i'!) \right]^{1/2} \quad (14)$$

$$\mathrm{H} = \sum_{k_{ij}=0}^{u_{ij}} \sum_{k_{ij}'=0}^{u_{ij}'} F_1 F_2 F_3 \quad (15)$$

where the explicit expression of each term not given above can be found elsewhere.[41] By squaring eq 12, one obtains the FCF.

Once the equilibrium geometries, vibrational frequencies, and normal modes of the two electronic states are obtained, the FCF corresponding to any vibronic transition can be computed using the above analytical expressions. To simulate the vibronic spectra, we take the FCF as the peak height, and each peak is given a Gaussian function to model its line shape. The contributions of all of the peaks are summed to construct the overall spectral profile. We also take the excitation energy of the adiabatic transition as the origin of the spectrum and plot the spectrum in a relative energy scale. In the harmonic model, the vibrational excitation energy, relative to the adiabatic transition, is computed using

$$\Delta E_v = \sum_{i=1}^{n} v_i \bar{\omega}_i \sum_{i=1}^{n} v_i' \bar{\omega}_i' \quad (16)$$

where $\bar{\omega}_i$ is the harmonic vibrational frequency (in cm^{-1}) of a given vibrational mode and the prime denotes the lower-lying electronic state. In the hybrid model, the anharmonic vibrational frequencies for the fundamental bands, first overtones, and combination bands of two fundamental transitions are taken from the Gaussian 16 computational outputs.[64] In Gaussian 16, the second-order perturbation theory (VPT2) is adopted for the anharmonic vibrational analysis,[65,66] in which the Fermi and Darling−Dennison resonances are taken into account by removing the resonant terms and then recovering them by variational correction.[65,66] The vibrational energies of other transitions are computed by

$$E_v = X_0 + \sum_{i=1}^{n} \left(v_i + \frac{1}{2} \right) \bar{\omega}_i + \sum_{i=1}^{n} \sum_{j=1}^{i} X_{ij} \left(v_i + \frac{1}{2} \right) \left(v_j + \frac{1}{2} \right) \quad (17)$$

where X_{ij}'s are the anharmonicity constants.

Quantum-Chemistry Computations. The equilibrium geometries, normal modes, and harmonic and anharmonic vibrational frequencies of MK and MK^+ were computed using the B3LYP, PBE0, APFD, and ωB97XD approaches of the density functional theory (DFT), associated with the basis set aug-cc-pVTZ (AVTZ). The Gaussian 16 programs were adopted for the quantum-chemistry computations of this work.[64] All of the optimized geometries correspond to equilibrium structures, judging from the fact that all vibrational frequencies have real positive values. The FCFs corresponding to the PES of $MK \rightarrow MK^+ + e^-$ were calculated using both the harmonic and hybrid models. The PES was simulated by using the computed FCFs and vibrational excitation energies. The full width at half-maximum (FWHM) of the Gaussian function was set to 10 cm^{-1} for the simulated spectrum with high resolutions, and was modified to 330 cm^{-1} for comparing the theoretical spectrum with the experimental PES recorded by Derbali et al.[12]

The adiabatic ionization energy (AIE) of MK was computed by using the CCSD(T) approach via extrapolating to the complete basis set (CBS) limit. At the B3LYP/AVTZ optimized geometries of MK and MK^+, single-point energies were calculated using the CCSD(T) approach in conjunction with the AVXZ (X = D, T, Q, 5) basis sets. The CCSD(T) energies were extrapolated to the CBS limit using six different formulas, i.e.,[57,67−70]

$$E(x) = E_{\mathrm{CBS}}1 + A\exp(-(x-1)) + B\exp(-(x-1)^2) \quad (18)$$

$$E(x) = E_{\mathrm{CBS}}2 + A\exp(-x) + B/(x-1)^2 \quad (19)$$

$$E(x) = E_{\mathrm{CBS}}3 + A\exp(-x) + B/(x-1)^3 \quad (20)$$

$$E(x) = E_{\mathrm{CBS}}4 + A\exp(-Bx) \quad (21)$$

$$E(x) = E_{\mathrm{CBS}}5 + A/x^B \quad (22)$$

$$E(x) = E_{\mathrm{CBS}}6 + A/(x+1/2)^4 + B/(x+1/2)^6 \quad (23)$$

where A and B are adjusting parameters, E_{CBS} is the CBS energy, and x = 2, 3, 4, 5 corresponding to the AVXZ (X = D, T, Q, 5) basis sets, respectively. We used six different CBS formulas because eqs 19 and 20 were developed by our group,[57] and we want to compare the performance of our formulas with the other four in predicting molecular properties involving energies. The AIE of MK was computed using

https://doi.org/10.1021/acsomega.3c05750
ACS Omega 2023, 8, 40685−40694

$$\mathrm{AIE} = E(\mathrm{MK}^+) + \mathrm{ZPE}(\mathrm{MK}^+) - E(\mathrm{MK}) - \mathrm{ZPE}(\mathrm{MK}) \quad (24)$$

where E is the CCSD(T) energy and ZPE is the vibrational zero-point energy obtained by the B3LYP/AVTZ computations. The harmonic and anharmonic ZPEs were adopted in calculating the AIE of MK when using the harmonic and hybrid models, respectively, in which the anharmonic ZPE was computed by[65]

$$\mathrm{ZPE} = X_0 + \frac{1}{2}\sum_{i=1}^{n}\left(\bar{\omega}_i + \frac{1}{2}X_{ii} + \sum_{j>i}X_{ij}\right) \quad (25)$$

Note that the computed E_{CBS} of MK^+ does not take into account the post triple excitation contributions, core correlation, spin−orbit correction, as well as relativistic and diagonal Born−Oppenheimer corrections. Consequently, the AIE computed using eq 24 is an approximation bearing the errors introduced by missing these corrections.

RESULTS AND DISCUSSION

Equilibrium Structures and Vibrational Frequencies.

Figure 1 depicts the structure and numbering of the atoms of

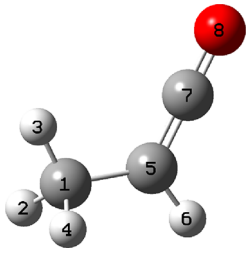

Figure 1. Structure and numbering of atoms of MK.

MK. Table 1 lists the equilibrium geometries of MK and MK^+ computed by B3LYP/AVTZ, and the results of the other three approaches can be found in Table S1. The differences of optimized geometries of MK and MK^+ between four computational approaches are marginal, and the computed geometries are consistent with the experimental values determined by Bak et al. using the microwave spectroscopy (Table 1).[14] The similar structures of MK and MK^+ render small values for the components of shift vector $\boldsymbol{D}$ (eq 5), in which the largest component is 0.138 amu$^{1/2}$ Å for ν_4. In addition, the diagonal elements of the Duschinsky matrix (eq 4) have absolute values close to 0.8 for ν_5 to ν_9 and larger than 0.9 for the rest, indicating that the mixing of vibrational wave functions within the FCI is only moderate.

Table 2 tabulates the harmonic and anharmonic vibrational frequencies of MK and MK^+, and the results of the other three approaches are provided in Tables S2 and S3. The calculated harmonic vibrational frequencies of MK are systematically larger than the experimental values determined by Winther et al. using the infrared spectroscopy (Table 2).[15] In contrast, the computed anharmonic vibrational frequencies of the fundamental bands of MK are in better agreement with the experimental values (Tables 2). The VPT2 approach might be performed poorly for hindered rotors, and the rotational barrier of the methyl group of MK is about 450 cm^{-1} computed by B3LYP/AVTZ. The corresponding mode for hindered rotation of MK is ν_{18}. The computed harmonic and anharmonic vibrational frequencies of ν_{18} for MK are 145 and

Table 1. Equilibrium Geometries of MK and MK^+

	B3LYP[b]		expt.[c]
parameter[a]	MK	MK^+	MK
R(C1,H2)	109.14	109.90	108.3
R(C1,H3)	108.87	108.52	108.3
R(C1,H4)	109.14	109.90	108.3
R(C1,C5)	151.01	147.39	151.8
R(C5,H6)	108.20	108.79	108.3
R(C5,C7)	130.82	137.43	130.6
R(C7,O8)	116.46	112.83	117.1
A(H2,C1,H3)	107.7	110.2	108.8
A(H2,C1,H4)	107.8	104.8	108.8
A(H2,C1,C5)	111.0	108.5	111.1
A(H3,C1,H4)	107.7	110.2	108.8
A(H3,C1,C5)	111.3	114.1	111.1
A(H4,C1,C5)	111.0	108.5	111.1
A(C1,C5,H6)	120.5	122.3	123.7
A(C1,C5,C7)	123.7	122.9	122.6
A(H6,C5,C7)	115.8	114.9	113.7
D(H2,C1,C5,H6)	−60.0	−56.7	
D(H2,C1,C5,C7)	120.0	123.3	
D(H3,C1,C5,H6)	180.0	180.0	
D(H3,C1,C5,C7)	0.0	0.0	
D(H4,C1,C5,H6)	60.0	56.7	
D(H4,C1,C5,C7)	−120.0	−123.3	

[a]R denotes the bond length (pm), A denotes the bond angle (degree), and D denotes the dihedral angle (degree). [b]Values computed by B3LYP/AVTZ. [c]Experimental geometries of MK determined by Bak et al.[14]

125 cm^{-1}, respectively, which are both in agreement with the experimental value of 135 cm^{-1} (Table 2), indicating that the VPT2 computation does not cause serious problems for the hindered rotation of MK. The anharmonic frequency of ν_{11} (651 cm^{-1}) for MK is nearly the same as its harmonic frequency (652 cm^{-1}), probably arising from the small cubic and quartic force constants and the Fermi resonance between ν_{11} and $\nu_{17} + \nu_{18}$. On the other hand, the anharmonic frequency of ν_{16} (582 cm^{-1}) for MK is higher than the harmonic frequency (554 cm^{-1}), which deserves some elaboration. There exists a Darling−Dennison resonance between ν_{16} and ν_{17}, and the frequencies of ν_{16} and ν_{17} prior to the Darling−Dennison correction are 544 and 502 cm^{-1}, respectively, which are close to the experimental values of 524 and 506 cm^{-1} (Table 2). However, they become 582 and 465 cm^{-1} after deperturbation and diagonalization, indicating that the extent of the Darling−Dennison resonance between ν_{16} and ν_{17} is not as large as computed.

We also list the anharmonic vibrational frequencies of MK^+ computed by Derbali et al. using the PBE0/AVTZ approach[12] in Table 2. Some of the anharmonic vibrational frequencies of MK^+ are not consistent between our and their computations. Comparing the PBE0 computations between the two studies, our calculated anharmonic frequency of ν_5 is 1420 cm^{-1} (Table S3), but the calculated value of ref 12 is 2298.1 cm^{-1} (Table 2). Similarly, ν_{13} values are computed to be 2869 and 1408.9 cm^{-1} in our and their studies, respectively. Such large deviations should not arise from computational errors between two independent researches. Rather, it is more likely to result from the problem of numbering the normal modes. We optimized the structures of MK and MK^+ under the C_s point group, and thus the symmetries and numbering of normal

https://doi.org/10.1021/acsomega.3c05750
ACS Omega 2023, 8, 40685−40694

Table 2. Harmonic and Anharmonic Vibrational Frequencies (cm^{-1}) of MK and MK^+ and the Experimental Vibrational Frequencies of MK

		MK	MK	MK	MK^+	MK^+	MK^+
mode	sym.[a]	harm.[b]	anharm.[b]	expt.[c]	harm.[b]	anharm.[b]	PBE0[d]
ν_1	A′	3176	3042	3073	3158	3027	3181.4
ν_2	A′	3105	2964	2988	3137	3001	3155.9
ν_3	A′	3023	2902	2923	2973	2808	3039.3
ν_4	A′	2197	2158	2136	2256	2225	2996.6
ν_5	A′	1512	1469	1477	1474	1422	2298.1
ν_6	A′	1422	1390	1389	1380	1341	1470.7
ν_7	A′	1411	1376	1369	1312	1278	1376.3
ν_8	A′	1154	1135	1132	1144	1114	1159.3
ν_9	A′	1084	1065	1079	1100	1075	1097.6
ν_{10}	A′	901	887	892	848	841	856.1
ν_{11}	A′	652	651	644	617	612	621.6
ν_{12}	A′	211	206	208	209	208	206.7
ν_{13}	A″	3068	2923	2964	3002	2829	1408.9
ν_{14}	A″	1485	1446	1452	1415	1363	1309.8
ν_{15}	A″	1060	1038	1092	942	917	931.9
ν_{16}	A″	554	582	524	671	660	667.8
ν_{17}	A″	515	465	506	444	438	451.4
ν_{18}	A″	145	125	135	118	95	119.3

[a]Symmetry species of the normal modes corresponding to the C_s point group. [b]Harmonic (harm.) and anharmonic (anharm.) vibrational frequencies computed by B3LYP/AVTZ. [c]Experimental vibrational frequencies measured by Winther et al.[15] [d]Anharmonic vibrational frequencies computed by Derbali et al. using the PBE0/AVTZ approach.[12]

modes should be correct. On the other hand, the structures of MK and MK^+ were optimized under the C_1 point group in ref 12, and the symmetry species of some normal modes might be determined incorrectly, such as interchanging the A′ and A″ species. Consequently, the numbering of normal modes might be different between our and their computations. However, the agreement of the symmetry species and vibrational frequencies of MK between our computations and the experimental data reported by Winther et al.[15] (Tables 2) supports that our numbering of normal modes is correct.

Photoelectron Spectrum and Adiabatic Ionization Energy. The simulated PES of MK using the harmonic and hybrid models is compared in Figure 2. The four DFT approaches predict similar spectral patterns. The peaks computed using the hybrid model (red) appear at the left of the corresponding peaks computed using the harmonic model (blue), manifesting the effect of anharmonic correction to the vibrational energies. The FCFs of the primary transitions are provided in Tables 3 and 4 for the harmonic and hybrid models, respectively.

In Figure 3, we compare the PES of MK simulated using the harmonic model with the experimental spectrum reported in ref 12. The agreement between the theoretical and experimental spectra is quite good, and the spectra simulated by using the four DFT approaches are almost identical (Figure 3b). However, our assignments (Figure 3b) are different from those made by ref 12 (Figure 3a). Aside from the origin band, the 8^1 band assigned by ref 12 is composed of the 9^1, 6^1, and 7^1 transitions according to the present study, as depicted in Figure 2. The 5^1 band of ref 12 is reassigned to 4^1 in this work (Figure 3), etc. The assignments of the bands between the two studies are compared in Table 5.

The inconsistency of spectral assignments made by us and by ref 12 arises from two sources. One is the problem of numbering normal modes, and the other is the distinction between the FA and SA approaches. If corrected for symmetry,

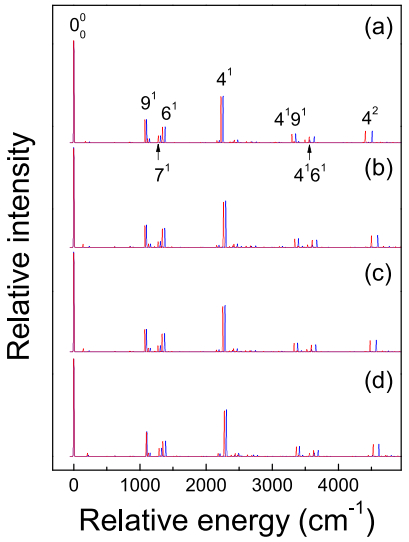

Figure 2. PES (FWHM = 10 cm^{-1}) of MK simulated using the B3LYP (a), PBE0 (b), APFD (c), and ωB97XD (d) approaches associated with the AVTZ basis set. The blue and red lines correspond to the harmonic and hybrid models, respectively.

ν_5 and ν_8 made by ref 12 should be renumbered as ν_4 and ν_7, respectively. Hereafter, we use the correct numbering to describe the assignments made by ref 12, and the corrected assignments are proposed in Table 5. Consequently, the assignment of the 9.214 eV band as 4^1 is consistent between the two studies. However, for the 9.083 eV band, it was assigned as 7^1 by ref 12 using the FA approach, but is assigned as the overlap of the 9^1, 6^1, and 7^1 transitions by us using the SA approach. Our assignments are based on the computed FCFs (Tables 3 and 4) and the simulated spectra (Figure 3b). Along the line of thinking of the FA, an observed band is most likely to arise from the transition whose excitation energy is

https://doi.org/10.1021/acsomega.3c05750
ACS Omega 2023, 8, 40685−40694

Table 3. FCFs of the Primary Transitions in the PES of MK Computed Using the Harmonic Model

B3LYP/AVTZ		PBE0/AVTZ		APFD/AVTZ		ωB97XD/AVTZ		
ΔE^a	FCF	ΔE	FCF	ΔE	FCF	ΔE	FCF	ionic state
0	3.6913×10^{-1}	0	3.6283×10^{-1}	0	3.6321×10^{-1}	0	3.5439×10^{-1}	0^0
1100	8.5504×10^{-2}	1097	8.1059×10^{-2}	1098	8.2328×10^{-2}	1105	9.0002×10^{-2}	9^1
1312	2.6375×10^{-2}	1309	2.1691×10^{-2}	1308	2.3173×10^{-2}	1329	2.9939×10^{-2}	7^1
1380	5.8215×10^{-2}	1376	6.9499×10^{-2}	1373	6.7284×10^{-2}	1389	5.6043×10^{-2}	6^1
2256	1.6980×10^{-1}	2298	1.6941×10^{-1}	2286	1.6894×10^{-1}	2306	1.6970×10^{-1}	4^1
3355	3.2891×10^{-2}	3396	3.1889×10^{-2}	3384	3.2173×10^{-2}	3411	3.6493×10^{-2}	$4^1 9^1$
3635	2.2295×10^{-2}	3674	2.7310×10^{-2}	3659	2.6282×10^{-2}	3695	2.2665×10^{-2}	$4^1 6^1$
4511	4.3194×10^{-2}	4596	4.3672×10^{-2}	4573	4.3397×10^{-2}	4613	4.5043×10^{-2}	4^2

[a] ΔE is the vibrational excitation energy (cm^{-1}) relative to the adiabatic ionization energy.

Table 4. FCFs of the Primary Transitions in the PES of MK Computed Using the Hybrid Model

B3LYP/AVTZ		PBE0/AVTZ		APFD/AVTZ		ωB97XD/AVTZ		
ΔE^a	FCF	ΔE	FCF	ΔE	FCF	ΔE	FCF	ionic state
0	3.7231×10^{-1}	0	3.5961×10^{-1}	0	3.5931×10^{-1}	0	3.5486×10^{-1}	0^0
1075	8.4601×10^{-2}	1075	7.9178×10^{-2}	1074	8.1614×10^{-2}	1096	8.8079×10^{-2}	9^1
1278	2.5900×10^{-2}	1274	2.1018×10^{-2}	1272	2.2300×10^{-2}	1289	2.9407×10^{-2}	7^1
1341	5.7423×10^{-2}	1338	6.7316×10^{-2}	1334	6.4995×10^{-2}	1346	5.4942×10^{-2}	6^1
2225	1.6827×10^{-1}	2263	1.6486×10^{-1}	2253	1.6424×10^{-1}	2275	1.6579×10^{-1}	4^1
3298	3.1842×10^{-2}	3341	3.0523×10^{-2}	3330	3.1628×10^{-2}	3365	3.4745×10^{-2}	$4^1 9^1$
3559	2.1435×10^{-2}	3604	2.5790×10^{-2}	3591	2.4712×10^{-2}	3626	2.1595×10^{-2}	$4^1 6^1$
4408	4.2512×10^{-2}	4500	4.2065×10^{-2}	4480	4.1588×10^{-2}	4527	4.3958×10^{-2}	4^2

[a] ΔE is the vibrational excitation energy (cm^{-1}) relative to the adiabatic ionization energy.

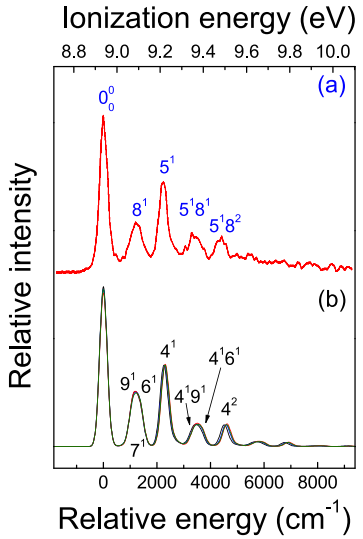

Figure 3. Experimental PES of MK reported by Derbali et al.[12] (a) and the spectra (FWHM = 330 cm^{-1}) simulated using the harmonic model (b). The spectra simulated using the B3LYP (black), PBE0 (green), APDF (blue), and ωB97XD (red) approaches are consistent with each other (b) and are also in harmony with the experimental spectrum. The assignments of bands in (a) are made by Derbali et al.,[12] and our assignments are provided in (b). The top axis corresponds to the ionization energy of the experimental spectrum. The experimental spectrum is reproduced from ref 12 with permission from the Royal Society of Chemistry.

closest to the experimental value. The assignment of the 9.083 eV band as 7^1 is a natural consequence, as made by ref 12. However, this approach is valid only when no overlap of spectral transitions occurs within the observed band, which cannot be known a priori from pure experimental measurements. Consequently, we propose that the SA approach is superior to the FA approach, given that the former provides both the information on intensities and excitation energies for assigning the spectrum, whereas the latter provides only the clue of excitation energies for assignments. The computed FCFs, taking the B3LYP hybrid model as examples hereafter, are 8.46×10^{-2}, 5.74×10^{-2}, and 2.59×10^{-2} for the 9^1, 6^1, and 7^1 transitions, respectively (Table 4). Therefore, it is unreasonable to assign this band as the weakest transition (7^1) of the three possible components. Similarly, the 9.360 eV band is primarily composed of $4^1 6^1$ and $4^1 9^1$ transitions, rather than the weaker $4^1 7^1$ transition (Table 4). In addition, the 9.484 eV band was assigned as $4^1 7^2$ by ref 12, albeit the possibility of 4^2 and $4^1 7^1 9^1$ transitions not being excluded. However, the FCF of 4^2 transition is much larger than those of $4^1 7^2$ and $4^1 7^1 9^1$, and thus it is more reasonable to assign this band as 4^2.

The vibrational structures of the PES can be further interpreted by scrutinizing the geometrical changes upon photoionization. If the neutral molecule and the cation have nearly the same equilibrium structures, the PES would be dominated by the origin band since its FCF, and hence the transition probability, is close to unity. On the other hand, the PES will consist of more vibrational excitations if the equilibrium geometry of the molecule changes appreciably upon ionization. The change of the geometries results in the displacement of the potential-energy surfaces between the two electronic states. Consequently, the relative FCFs for the vibrational excitations are greater because of the greater overlap of vibrational wave functions. The four normal modes dominate the vibrational structures of the PES of MK are depicted in Figure 4. The ν_4 mode corresponds to C═C═O asymmetric stretching, ν_6 CH_3 deformation, ν_7 CH_2 bending, and ν_9 C═C−H bending (Figure 4). Taking the B3LYP computations as examples, the largest change of bond lengths between MK^+ and MK occurs at R(C═C) (+6.61 pm) and R(C═O) (−3.63 pm), leading to the strong ν_4 excitation of

https://doi.org/10.1021/acsomega.3c05750
ACS Omega 2023, 8, 40685−40694

Table 5. Assignment and Mean Absolute Error (MAE) of Excitation Energy for the PES of MK

band (eV)[a]	8.937	9.083	9.214	9.360	9.484	MAE[b]
ΔE(expt.)[a]	0.0	1177.6	2234.1	3411.7	4411.8	
ΔE(PBE0)[a]	0.0	1159.3	2298.1	3457.1	4616.7	66.5
harmonic model[c]						
ΔE(B3LYP)	0	1186	2260	3445	4514	34.0
ΔE(PBE0)	0	1226	2302	3532	4599	106.0
ΔE(APFD)	0	1217	2291	3510	4576	71.8
ΔE(ωB97XD)	0	1190	2310	3500	4616	76.2
hybrid model[c]						
ΔE(B3LYP)	0	1165	2230	3391	4412	7.5
ΔE(PBE0)	0	1199	2270	3466	4506	41.1
ΔE(APFD)	0	1186	2262	3443	4488	28.8
ΔE(ωB97XD)	0	1188	2281	3460	4533	45.4
assignment						
ref 12[a]	0°	8^1	5^1	$5^1 8^1$	$5^1 8^2/5^2/5^1 8^1 9^1$	
ref 12[d]	0°	7^1	4^1	$4^1 7^1$	$4^1 7^2/4^2/4^1 7^1 9^1$	
this work	0°	$6^1+7^1+9^1$	4^1	$4^1 6^1+4^1 9^1$	4^2	

[a]Taken from ref 12. [b]The MAE of excitation energy corresponding to band maxima. [c]Values analyzed from the harmonic or hybrid model of this work. [d]The assignments of ref 12 if the symmetries are corrected (see text).

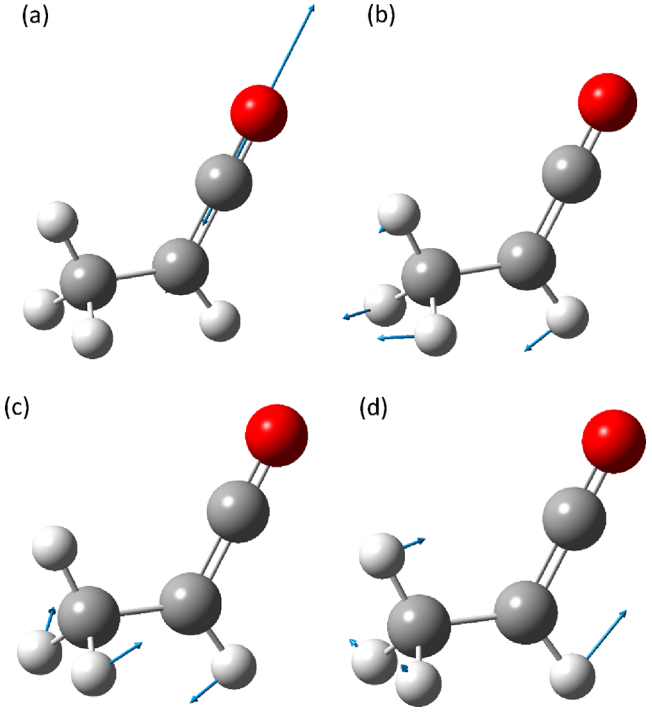

Figure 4. Normal modes of ν_4 (a), ν_6 (b), ν_7 (c), and ν_9 (d) of MK^+ responsible for the primary transitions in the PES of MK, computed by B3LYP/AVTZ.

the C═C═O asymmetric stretching. The C═C bond elongates, whereas the C═O bond shortens upon ionization, because the former has bonding characters, while the latter has antibonding characters, as demonstrated by the highest occupied molecular orbital of MK (Figure 5). The bond angles and dihedral angles involving the H atoms also change slightly (within 3.3°) upon ionization, accounting for the excitations of ν_9, ν_7, and ν_6.

We compare the PES simulated using the hybrid model with the experimental spectrum[12] in Figure 6, in which the experimental spectrum is reassigned based on the SA approach. The agreement between the theoretical and experimental

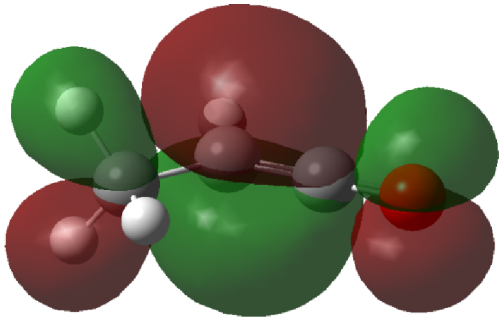

Figure 5. Highest occupied molecular orbital of MK for the structure optimized by B3LYP/AVTZ.

spectra is as good as the harmonic model (Figure 3). However, the hybrid model performs better in predicting the excitation energies, as indicated by the vertical arrow for the 4^2 band in Figure 6. More precisely, we computed the mean absolute error (MAE) of the excitation energy for band maxima. Here, the excitation energy is defined as the energy of a band relative to the AIE. Even for an overlapped band, such as the 9.083 eV band, both the simulated and experimental spectra show a single band maximum (Figure 6). Accordingly, by analysis of the band maxima, the performance of a theoretical spectrum can be evaluated by its MAE of excitation energy with respect to the experimental spectrum. Note that the excitation energy of a band maximum needs not be the same as that of any of the vibrational modes or their combinations, particularly for overlapped bands. For example, the band maximum of the 9.083 eV band appears at 1177.6 cm^{-1} (1165 cm^{-1} computed; Table 5), but the corresponding modes possess vibrational energies of 1075, 1278, and 1341 cm^{-1} for the 9^1, 7^1, and 6^1 transitions (Table 5), respectively. On the other hand, the excitation energy of a band maximum will be close to the vibrational energy of the corresponding mode if the overlap of bands is not severe. For example, the computed band maxima appear at 2230 and 4412 cm^{-1} for the 4^1 and 4^2 transitions (Table 5), respectively, only slightly deviated from 2225 and 4408 cm^{-1} of their vibrational energies (Table 4).

By inspection of Table 5, it can be seen that the MAEs of excitation energy of the hybrid model are all smaller than those

https://doi.org/10.1021/acsomega.3c05750
ACS Omega 2023, 8, 40685−40694

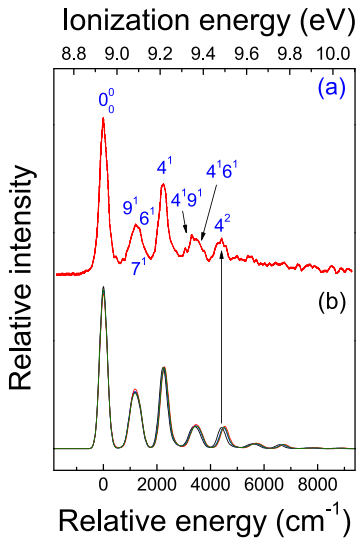

Figure 6. Experimental PES of MK reported by Derbali et al.[12] (a) and the spectra (FWHM = 330 cm^{-1}) simulated using the hybrid model (b). The spectra simulated using the B3LYP (black), PBE0 (green), APDF (blue), and ωB97XD (red) approaches are consistent with each other (b) and are also in harmony with the experimental spectrum. The top axis corresponds to the ionization energy of the experimental spectrum. The experimental spectrum (a) is reassigned using the SA approach. The experimental spectrum is reproduced from ref 12 with permission from the Royal Society of Chemistry.

of the harmonic model for the four DFT approaches. The B3LYP/AVTZ computation gives the smallest MAEs of excitation energy, which are 34.0 and 7.5 cm^{-1} for the harmonic and hybrid models, respectively. The MAEs of excitation energy of our hybrid model, distributed from 7.5 to 45.4 cm^{-1}, are also smaller than that of the anharmonic computations of ref 12 (66.5 cm^{-1}; Table 5).

Although the simulated PES of MK agrees with the experiment quite well, the relative intensity of the 9.083 eV band is overestimated by the theoretical spectrum (Figure 6). A possible reason is that the wave functions of the corresponding vibrational states (ν_9, ν_7, and ν_6) for computing FCFs are not accurate enough, albeit the computation indicating that there is a high overlap with the state to which it is assigned, for any of the three states. The ν_9 mode undergoes Fermi resonances with $\nu_{16} + \nu_{17}$ and $2\nu_{16}$, meaning that the wave function of ν_9 should be mixed with those of $\nu_{16} + \nu_{17}$ and $2\nu_{16}$. In addition, there exists Darling–Dennison resonance between ν_6 and ν_7, and their wave functions must be mixed, too. The computation of FCFs using the vibrational wave functions corrected for the Fermi and Darling–Dennison resonances is beyond the scope of the present study but should be an interesting issue and will be explored in the future.

The AIEs of MK computed using the CCSD(T) approach are provided in Table 6, together with the experimental value (8.937 eV) determined by Derbali et al.[12] The error of computed AIE decreases as the level of basis sets elevated from AVDZ to AV5Z, and it is even smaller for the CBS limit. The error of $E_{CBS}5$ is the smallest (−0.017 eV) of the six CBS formulas adopted and is also smaller than that (−0.020 eV) computed using the CCSD(T)-F12 approach by Derbali et al.[12] Our CBS formulas, eqs 21 and 22, also provide accurate predictions for the AIE of MK, with the errors being −0.019 and −0.024 eV for $E_{CBS}2$ and $E_{CBS}3$ (Table 6), respectively.

Table 6. CCSD(T) Energies (in Hartree) and Adiabatic Ionization Energy (AIE) of MK

method	MK	MK^+	AIE (eV)	error (eV)
CCSD(T)/AVDZ	−191.44016966	−191.12040955	8.672	−0.265
CCSD(T)/AVTZ	−191.60972798	−191.28358168	8.846	−0.091
CCSD(T)/AVQZ	−191.65805749	−191.33032248	8.889	−0.048
CCSD(T)/AV5Z	−191.67274268	−191.34446633	8.904	−0.033
$E_{CBS}1$[a]	−191.68296094	−191.35437163	8.912	−0.025
$E_{CBS}2$	−191.68744585	−191.35863718	8.918	−0.019
$E_{CBS}3$	−191.68333836	−191.35473094	8.913	−0.024
$E_{CBS}4$	−191.67821913	−191.34983093	8.907	−0.030
$E_{CBS}5$	−191.69468198	−191.36581682	8.920	−0.017
$E_{CBS}6$	−191.68738773	−191.35866823	8.916	−0.021
CCSD(T)-F12[b]			8.917	−0.020
experiment[b]			8.937	

[a] E_{CBS} is the CCSD(T) energies extrapolated to the CBS limit using eqs 18–23 (see text). [b] Taken from ref 12.

CONCLUSIONS

A hybrid model of harmonic and anharmonic oscillators was developed to compute FCFs and simulate the vibronic spectra of molecules. The PES of MK were simulated using both the harmonic and hybrid models and are compared with the experimental spectrum recorded by Derbali et al.[12] Although the harmonic and hybrid models perform equally well in predicting the spectral patterns, the hybrid model provides more accurate excitation energies for the PES of MK. The AIEs of MK computed using the CCSD(T) approach extrapolated to the CBS limit are in agreement with the experimental value, with the smallest error being −0.017 eV.

The experimental PES of MK was reassigned based on the SA approach. We propose that the SA approach is superior to the FA approach in interpreting the vibrational structures of a vibronic spectrum. In the SA approach, both the information on intensities and excitation energies are compared with the experiments, whereas the FA approach is based solely on the excitation energies. Envisioning from experimental viewpoints, it would be interesting to acquire the PES of MK with higher resolutions or to record the infrared emission spectra of the photoions of MK, such that the conclusions of this study can be further verified.

ASSOCIATED CONTENT

Supporting Information

The Supporting Information is available free of charge at https://pubs.acs.org/doi/10.1021/acsomega.3c05750.

Optimized structures, harmonic and anharmonic vibrational frequencies computed by the four DFT approaches (PDF)

AUTHOR INFORMATION

Corresponding Author

Jia-Lin Chang − *Department of Science Education and Application, National Taichung University of Education, Taichung 403514, Taiwan, Republic of China;* orcid.org/0000-0003-3038-0174; Email: jlchang@mail.ntcu.edu.tw

https://doi.org/10.1021/acsomega.3c05750
ACS Omega 2023, 8, 40685−40694

Authors

Hsiang-Yu Chen − *Department of Science Education and Application, National Taichung University of Education, Taichung 403514, Taiwan, Republic of China*

Yun-Jhu Huang − *Department of Science Education and Application, National Taichung University of Education, Taichung 403514, Taiwan, Republic of China*

Complete contact information is available at: https://pubs.acs.org/10.1021/acsomega.3c05750

Notes

The authors declare no competing financial interest.

■ ACKNOWLEDGMENTS

This work is supported by the National Science and Technology Council of the Republic of China (grant no. NSTC 112-2113-M-142-002).

■ REFERENCES

(1) Turner, B. E. Microwave detection of interstellar ketene. *Astrophys. J.* **1977**, *213*, L75−L79.

(2) Bermúdez, C.; Tercero, B.; Motiyenko, R. A.; Margulès, L.; Cernicharo, J.; Ellinger, Y.; Guillemin, J.-C. The millimeter-wave spectrum of methyl ketene and the astronomical search for it. *Astron. Astrophys.* **2018**, *619*, A92.

(3) Karton, A.; Talbi, D. Pinning the most stable $H_xC_yO_z$ isomers in space by means of high-level theoretical procedures. *Chem. Phys.* **2014**, *436*−*437*, 22−28.

(4) Field-Theodore, T. E.; Taylor, P. R. Interstellar hide and go seek: C_3H_4O. There and back (again). *Phys. Chem. Chem. Phys.* **2022**, *24* (32), 19184−19198.

(5) Hollis, J. M.; Jewell, P. R.; Lovas, F. J.; Remijan, A.; Møllendal, H. Green Bank Telescope Detection of New Interstellar Aldehydes: Propenal and Propanal. *Astrophys. J.* **2004**, *610* (1), L21−L24.

(6) Requena-Torres, M. A.; Martin-Pintado, J.; Martin, S.; Morris, M. R. The galactic center: The largest oxygen-bearing organic molecule repository. *Astrophys. J.* **2008**, *672* (1), 352−360.

(7) Manigand, S.; Coutens, A.; Loison, J. C.; Wakelam, V.; Calcutt, H.; Müller, H. S. P.; Jørgensen, J. K.; Taquet, V.; Wampfler, S. F.; Bourke, T. L.; Kulterer, B. M.; van Dishoeck, E. F.; Drozdovskaya, M. N.; Ligterink, N. F. W. The ALMA-PILS survey: first detection of the unsaturated 3-carbon molecules Propenal (C2H3CHO) and Propylene (C3H6) towards IRAS 16293−2422 B. *Astron. Astrophys.* **2021**, *645*, A53 DOI: 10.1051/0004-6361/202038113.

(8) Agúndez, M.; Marcelino, N.; Tercero, B.; Cabezas, C.; de Vicente, P.; Cernicharo, J. O-bearing complex organic molecules at the cyanopolyyne peak of TMC-1: Detection of C_2H_3CHO, C_2H_3OH, $HCOOCH_3$, and CH_3OCH_3. *Astron. Astrophys.* **2021**, *649*, L4 DOI: 10.1051/0004-6361/202140978.

(9) Lattelais, M.; Pauzat, F.; Ellinger, Y.; Ceccarelli, C. Interstellar complex organic molecules and the minimum energy principle. *Astrophys. J.* **2009**, *696* (2), L133.

(10) Lattelais, M.; Pauzat, F.; Ellinger, Y.; Ceccarelli, C. A new weapon for the interstellar complex organic molecule hunt: the minimum energy principle. *Astron. Astrophys.* **2010**, *519*, A30 DOI: 10.1051/0004-6361/200913869.

(11) Lattelais, M.; Bertin, M.; Mokrane, H.; Romanzin, C.; Michaut, X.; Jeseck, P.; Fillion, J. H.; Chaabouni, H.; Congiu, E.; Dulieu, F.; Baouche, S.; Lemaire, J.-L.; Pauzat, F.; Pilmé, J.; Minot, C.; Ellinger, Y. Differential adsorption of complex organic molecules isomers at interstellar ice surfaces. *Astron. Astrophys.* **2011**, *532*, A12 DOI: 10.1051/0004-6361/201016184.

(12) Derbali, I.; Hrodmarsson, H. R.; Schwell, M.; Bénilan, Y.; Poisson, L.; Hochlaf, M.; Alikhani, M. E.; Guillemin, J.-C.; Zins, E.-L. Unimolecular decomposition of methyl ketene and its dimer in the gas phase: theory and experiment. *Phys. Chem. Chem. Phys.* **2020**, *22* (36), 20394−20408.

(13) Bak, B.; Christensen, D.; Christiansen, J.; Hansen-Nygaard, L.; Rastrup-Andersen, J. Microwave spectrum and internal barrier of rotation of methyl ketene. *Spectrochim. Acta* **1962**, *18* (11), 1421−1424.

(14) Bak, B.; Christiansen, J. J.; Kunstmann, K.; Nygaard, L.; Rastrup-Andersen, J. Microwave Spectrum, Molecular Structure, Barrier to Internal Rotation, and Dipole Moment of Methylketene. *J. Chem. Phys.* **1966**, *45* (3), 883−887.

(15) Winther, F.; Meyer, S.; Nicolaisen, F. M. The infrared spectrum of methylketene. *J. Mol. Struct.* **2002**, *611* (1), 9−22.

(16) Bock, H.; Hirabayashi, T.; Mohmand, S. Gasphasen-Reaktionen, 21. Thermische Erzeugung von Alkyl- und Halogen-ketenen. *Chem. Ber.* **1981**, *114* (7), 2595−2608.

(17) Cyvin, S. J.; Christensen, D. H.; Nielsen, O. F. Mean amplitudes of vibration for methyl ketene. *Chem. Phys. Lett.* **1970**, *5* (9), 597−600.

(18) McKee, M. L.; Radom, L. Structures and stabilities of $C_3H_4O^{+\cdot}$ isomers: A G2 theoretical study. *Org. Mass Spectrom.* **1993**, *28* (10), 1238−1244.

(19) Fang, W.-H. A CASSCF study on photodissociation of acrolein in the gas phase. *J. Am. Chem. Soc.* **1999**, *121* (36), 8376−8384.

(20) Chin, C.-H.; Lee, S.-H. Theoretical study of isomerization and decomposition of propenal. *J. Chem. Phys.* **2011**, *134* (4), No. 044309.

(21) Pham, T. V.; Tue Trang, H. T. Combination reactions of propargyl radical with hydroxyl radical and the isomerization and dissociation of trans-propenal. *J. Phys. Chem. A* **2020**, *124* (30), 6144−6157.

(22) Kistiakowsky, G. B.; Mahan, B. H. Stability of ethylidene radicals. *J. Chem. Phys.* **1956**, *24* (4), 922−922.

(23) Kistiakowsky, G. B.; Mahan, B. H. The photolysis of methyl ketene. *J. Am. Chem. Soc.* **1957**, *79* (10), 2412−2419.

(24) Chong, D. P.; Kistiakowsky, G. B. The photolysis of methylketenem II. *J. Phys. Chem.* **1964**, *68* (7), 1793−1797.

(25) Umstead, M. E.; Shortridge, R. G.; Lin, M. C. Energy partitioning in the photodissociation of C_3H_4O near 200 nm. *J. Phys. Chem.* **1978**, *82* (13), 1455−1460.

(26) Fujimoto, G. T.; Umstead, M. E.; Lin, M. C. CO product energy distribution in the photodissociation of methylketene and acrolein at 193 nm. *J. Chem. Phys.* **1985**, *82* (7), 3042−3044.

(27) Hutchisson, E. Band Spectra Intensities for Symmetrical Diatomic Molecules. *Phys. Rev.* **1930**, *36* (3), 410−420.

(28) Manneback, C. Computation of the intensities of vibrational spectra of electronic bands in diatomic molecules. *Physica* **1951**, *17* (11), 1001−1010.

(29) Wagner, M. Exakte Berechnung von Franck-Condon-Integralen. *Z. Naturforsch. A* **1959**, *14* (1), 81−91.

(30) Ansbacher, F. A note on the overlap integral of two harmonic oscillator wave functions. *Z. Naturforsch. A* **1959**, *14A*, 889−892.

(31) Chang, J.-L. A new formula to calculate Franck−Condon factors for displaced and distorted harmonic oscillators. *J. Mol. Spectrosc.* **2005**, *232* (1), 102−104.

(32) Duschinsky, F. On the Interpretation of Electronic Spectra of Polyatomic Molecules. *Acta Physicochim. URSS* **1937**, *7*, 551−566.

(33) Sharp, T. E.; Rosenstock, H. M. Franck—Condon Factors for Polyatomic Molecules. *J. Chem. Phys.* **1964**, *41* (11), 3453−3463.

(34) Doktorov, E. V.; Malkin, I. A.; Man'ko, V. I. Dynamical symmetry of vibronic transitions in polyatomic molecules and the Franck-Condon principle. *J. Mol. Spectrosc.* **1975**, *56* (1), 1−20.

(35) Toniolo, A.; Persico, M. Efficient calculation of Franck−Condon factors and vibronic couplings in polyatomics. *J. Comput. Chem.* **2001**, *22* (9), 968−975.

(36) Hazra, A.; Nooijen, M. Derivation and efficient implementation of a recursion formula to calculate harmonic Franck−Condon factors for polyatomic molecules. *Int. J. Quantum Chem.* **2003**, *95* (4−5), 643−657.

(37) Dierksen, M.; Grimme, S. An efficient approach for the calculation of Franck−Condon integrals of large molecules. *J. Chem. Phys.* **2005**, *122* (24), No. 244101.

(38) Mebel, A. M.; Hayashi, M.; Liang, K. K.; Lin, S. H. Ab Initio Calculations of Vibronic Spectra and Dynamics for Small Polyatomic Molecules: Role of Duschinsky Effect. *J. Phys. Chem. A* **1999**, *103* (50), 10674−10690.
(39) Kikuchi, H.; Kubo, M.; Watanabe, N.; Suzuki, H. Computational method for calculating multidimensional Franck−Condon factors: Based on Sharp−Rosenstock's method. *J. Chem. Phys.* **2003**, *119* (2), 729−736.
(40) Barone, V.; Bloino, J.; Biczysko, M.; Santoro, F. Fully Integrated Approach to Compute Vibrationally Resolved Optical Spectra: From Small Molecules to Macrosystems. *J. Chem. Theory Comput.* **2009**, *5* (3), 540−554.
(41) Chang, J.-L.; Huang, C.-H.; Chen, S.-C.; Yin, T.-H.; Chen, Y.-T. An analytical approach for computing Franck-Condon integrals of harmonic oscillators with arbitrary dimensions. *J. Comput. Chem.* **2013**, *34* (9), 757−765.
(42) Sattasathuchana, T.; Murri, R.; Baldridge, K. K. An Efficient Analytic Approach for Calculation of Multi-Dimensional Franck−Condon Factors and Associated Photoelectron Spectra. *J. Chem. Theory Comput.* **2017**, *13* (5), 2147−2158.
(43) Herzberg, G.; Teller, E. Fluctuation structure of electron transfer in multiatomic molecules. *Z. Phys. Chem. B* **1933**, *21*, 410.
(44) Bloino, J.; Biczysko, M.; Santoro, F.; Barone, V. General Approach to Compute Vibrationally Resolved One-Photon Electronic Spectra. *J. Chem. Theory Comput.* **2010**, *6* (4), 1256−1274.
(45) Baiardi, A.; Bloino, J.; Barone, V. General Time Dependent Approach to Vibronic Spectroscopy Including Franck−Condon, Herzberg−Teller, and Duschinsky Effects. *J. Chem. Theory Comput.* **2013**, *9* (9), 4097−4115.
(46) Carvajal, M.; Arias, J. M.; Gómez-Camacho, J. Analytic evaluation of Franck-Condon integrals for anharmonic vibrational wave functions. *Phys. Rev. A* **1999**, *59* (5), 3462−3470.
(47) Mok, D. K. W.; Lee, E. P. F.; Chau, F.-T.; Wang, D.; Dyke, J. M. A new method of calculation of Franck−Condon factors which includes allowance for anharmonicity and the Duschinsky effect: Simulation of the He I photoelectron spectrum of ClO2. *J. Chem. Phys.* **2000**, *113* (14), 5791−5803.
(48) Rodriguez-Garcia, V.; Yagi, K.; Hirao, K.; Iwata, S.; Hirata, S. Franck-Condon factors based on anharmonic vibrational wave functions of polyatomic molecules. *J. Chem. Phys.* **2006**, *125* (1), No. 014109.
(49) Petrenko, T.; Rauhut, G. A General Approach for Calculating Strongly Anharmonic Vibronic Spectra with a High Density of States: The $\tilde{X}^2B_1^-$ $\tilde{X}^1A_1$ Photoelectron Spectrum of Difluoromethane. *J. Chem. Theory Comput.* **2017**, *13* (11), 5515−5527.
(50) Bloino, J.; Baiardi, A.; Biczysko, M. Aiming at an accurate prediction of vibrational and electronic spectra for medium-to-large molecules: An overview. *Int. J. Quantum Chem.* **2016**, *116* (21), 1543−1574.
(51) Luis, J. M.; Bishop, D. M.; Kirtman, B. A different approach for calculating Franck−Condon factors including anharmonicity. *J. Chem. Phys.* **2004**, *120* (2), 813−822.
(52) Chang, J.-L. A new method to calculate Franck−Condon factors of multidimensional harmonic oscillators including the Duschinsky effect. *J. Chem. Phys.* **2008**, *128* (17), 174111.
(53) Lee, C.-L.; Yang, S.-H.; Kuo, S.-Y.; Chang, J.-L. A general formula of two-dimensional Franck−Condon integral and the photoelectron spectroscopy of sulfur dioxide. *J. Mol. Spectrosc.* **2009**, *256* (2), 279−286.
(54) Huang, C.-H.; Chou, S.-Y.; Jang, S.-B.; Lin, Y.-C.; Li, C.-E.; Chen, C.-C.; Chang, J.-L. Insights into the Photoelectron Spectroscopy of Chlorofluoroethenes Studied by Density-Functional and Coupled-Cluster Theories. *J. Phys. Chem. A* **2016**, *120* (8), 1175−1183.
(55) Chang, J.-L.; Wang, Y.-C.; Chang, M.-F.; Huang, Y.-J. Prediction of the photoelectron spectra of C_{122} by computing Franck-Condon factors. *AIP Adv.* **2019**, *9* (6), No. 065114.
(56) Huang, C.-H.; Chen, C.-C.; Chen, Y.-K.; Tsai, S.-C.; Chang, J.-L. A theoretical study on the equilibrium structures, vibrational frequencies and photoelectron spectroscopy of thiocarbonyl fluoride by using density functional and coupled-cluster theories. *Chem. Phys.* **2014**, *440* (Supplement C), 99−105.
(57) Chang, J.-L.; Hsieh, J.-H.; Huang, Y.-J.; Chen, C.-C.; Chang, M.-F. A theoretical study of the photoelectron spectra of dichloroketene with accurate computation of ionization energies via complete basis set limit extrapolation. *Int. J. Quantum Chem.* **2019**, *119* (8), No. e25866.
(58) Chang, J.-L.; Jen, C.-C.; Huang, Y.-J.; Du, Z.-K. Distinction of photoelectron spectroscopy of cis- and trans-acrolein explored by theoretical computation. *Chem. Phys.* **2021**, *546*, No. 111166.
(59) Chang, J.-L.; Kuo, W.-H.; Huang, Y.-J.; Chang, M.-F.; Huang, J.-Y.; Chen, L.-W. Identification of the photoelectron spectra of HFCS via computing Franck−Condon factors. *Comput. Theor. Chem.* **2021**, *1204*, No. 113393.
(60) Bloino, J.; Biczysko, M.; Crescenzi, O.; Barone, V. Integrated computational approach to vibrationally resolved electronic spectra: Anisole as a test case. *J. Chem. Phys.* **2008**, *128* (24), 244105.
(61) Biczysko, M.; Bloino, J.; Barone, V. First principle simulation of vibrationally resolved $A^2B_1\tilde{X}^2A_1$ electronic transition of phenyl radical. *Chem. Phys. Lett.* **2009**, *471* (1), 143−147.
(62) Egidi, F.; Bloino, J.; Cappelli, C.; Barone, V. A Robust and Effective Time-Independent Route to the Calculation of Resonance Raman Spectra of Large Molecules in Condensed Phases with the Inclusion of Duschinsky, Herzberg−Teller, Anharmonic, and Environmental Effects. *J. Chem. Theory Comput.* **2014**, *10* (1), 346−363.
(63) Egidi, F.; Williams-Young, D. B.; Baiardi, A.; Bloino, J.; Scalmani, G.; Frisch, M. J.; Li, X.; Barone, V. Effective inclusion of mechanical and electrical anharmonicity in excited electronic states: VPT2-TDDFT route. *J. Chem. Theory Comput.* **2017**, *13* (6), 2789−2803.
(64) Frisch, M. J.; Trucks, G. W.; Schlegel, H. B.; Scuseria, G. E.; Robb, M. A.; Cheeseman, J. R.; Scalmani, G.; Barone, V.; Petersson, G. A.; Nakatsuji, H. et al.*Gaussian 16, Revision A.03*; Gaussian, Inc.: Wallingford CT, 2016.
(65) Barone, V. Anharmonic vibrational properties by a fully automated second-order perturbative approach. *J. Chem. Phys.* **2005**, *122* (1), No. 014108.
(66) Bloino, J.; Barone, V. A second-order perturbation theory route to vibrational averages and transition properties of molecules: General formulation and application to infrared and vibrational circular dichroism spectroscopies. *J. Chem. Phys.* **2012**, *136* (12), No. 124108.
(67) Peterson, K. A.; Woon, D. E.; Dunning, T. H. Benchmark calculations with correlated molecular wave functions. IV. The classical barrier height of the $H+H_2\rightarrow H_2+H$ reaction. *J. Chem. Phys.* **1994**, *100* (10), 7410−7415.
(68) Feller, D. The use of systematic sequences of wave functions for estimating the complete basis set, full configuration interaction limit in water. *J. Chem. Phys.* **1993**, *98* (9), 7059−7071.
(69) Helgaker, T.; Klopper, W.; Koch, H.; Noga, J. Basis-set convergence of correlated calculations on water. *J. Chem. Phys.* **1997**, *106* (23), 9639−9646.
(70) Martin, J. M. L. Ab initio total atomization energies of small molecules — towards the basis set limit. *Chem. Phys. Lett.* **1996**, *259* (5), 669−678.

https://doi.org/10.1021/acsomega.3c05750
ACS Omega 2023, 8, 40685−40694